Bidentate Ligand-Induced Oriented Transformation of $CsPbBr_3$ Perovskite Nanocrystals into Nanowires for X-ray Photodetectors

Chunyu Zhao,[†] Zaozhen He,[†]Peihua Wangyang,[‡] Jie Tan,[‡] Chengyu Shi,[†] Aizhao Pan,[*,†] Ling He,[†] Yi Liu[*,#]

† School of Chemistry, Xi'an Jiaotong University, Xianning West Road, 28, Xi'an, 710049, China.

‡ Guangxi Key Laboratory of Precision Navigation Technology and Application, Guilin University of Electronic Technology, Guilin, 541004, China

The Molecular Foundry and Materials Sciences Division, Lawrence Berkeley National Laboratory, Berkeley, California 94720, United States.

Corresponding Authors

*Email: panaizhao2017032@xjtu.edu.cn; yliu@lbl.gov.

KEYWORDS: anisotropic growth; bidentate ligands; $CsPbX_3$ nanocrystal; nanowires; ; X-ray photodetector

Abstract:

Shape and dimensionality control by ligands is an efficient way to fabricate high-quality perovskite nanocrystals (NCs) with optoelectronic properties. Herein, to realize oriented transformations between different morphologies of $CsPbBr_3$ nanocrystals, we conceived the use of defects and bidentate ligands to synergistically drive the reorientation of $CsPbBr_3$ nanocrystals into $CsPbBr_3$ nanowires (NWs). Employing aminocaproic acid as the bidentate ligand, $CsPbBr_3$ NWs were reconstructed from the $CsPbBr_3$ NCs (~7 nm) with 20–60 nm in width and several micrometers in length, as well as a 527 nm photoluminescence (PL) peak, 59% PL quantum yield, and 98.5 ns PL lifetime. The bidentate ligand-directed anisotropic shape evolution and growth of perovskite NWs from NCs was elucidated by transmission electronmicroscopy and PL studies. The photodetectors fabricated with the reconstructed $CsPbBr_3$ NWs displayed a photocurrent enhancement (2.75×10^{-11} A) compared with that of the devices based on solution-synthesized NWs (2.28×10^{-11} A). The device also showed a short response time, indicating its more sensitive photoelectric response. This process provides a viable approach to engineering diverse morphologies of perovskite nanocrystals for optoelectronic applications.

INTRODUCTION

As a recent entry into the perovskite nanocrystal family, all-inorganic lead halide $CsPbX_3$ (X = Cl, Br, I) perovskite nanocrystals (NCs) have manifested promising candidates for next-generation optoelectronic devices, such as multicolor light-emitting diodes (LEDs), photodetectors, lasers, and photovoltaic cells.[1-5] Their encouraging properties have fueled growing needs for more detailed studies in order to fully understand and improve their optoelectronic characteristics. Great efforts have been contributed to improve the optoelectronic

efficiencies, decrease the spectral widths, improve the colloidal dispersibility, and tune the bandgaps of these materials.[6-10]

Beyond compositional variations, considerable progress has been achieved in controlling colloidal perovskite particle dimensions and morphologies, such as nanocubes, nanowires (NWs) and nanoplatelets (NPLs), by regulating the ligands, temperature, and precursors.[6, 11-14] As commonly used ligands in the synthesis of colloidal perovskite NCs, long-chain oleic acid (OA) and oleylamine (OAm) can effectively solvate inorganic precursors, regulate the kinetic pathways to generate anisotropically developed nanostructures, and stabilize the final NCs.[1, 14-15] De Roo *et al.* demonstrated that the surface of perovskite nanocrystals were dynamically capped with either oleylammonium bromide or oleylammonium oleate.[15] The low formation energy and the ionic nature of $CsPbX_3$ NCs make the surface ligands very labile and sensitive to the external environment.[16-19] The dynamic ligands also render it feasible to regulate the crystal facet growth to obtain perovskite NCs with diverse morphologies and optical properties.[19-22]

The dimension-dependent properties of perovskite NCs are expected to show diverse carrier diffusion lengths, light-trapping, and mechanical properties, all relevant for future perovskite-based nanoscale optoelectronic and photonic devices.[20, 22-24] However, investigations into the conversion between different dimensional perovskite nanostructures are rather limited. Among the diverse morphologies of $CsPbX_3$, one-dimensional (1D) $CsPbX_3$ perovskite NWs have several merits, including good crystallinity, high aspect ratios, strong light absorption, and long carrier migration lengths.[23, 25-27] Currently, many efforts to study the synthesis of $CsPbBr_3$ nanowires (NWs) have been reported, including solution-based synthesis, solvent evaporation-induced recrystallization, chemical vapor deposition, and polar solvent, visible light, or ultrasound-induced transformations from NCs.[20-21, 23, 25-28] Despite the successful formation of $CsPbBr_3$ NWs, the relationship between the ligands and the NW size,

shape, and optical properties remains poorly understood, thus calling for a more detailed structure-morphology-property study. Herein, we propose a new approach to transforming $CsPbBr_3$ NCs into NWs using the bidentate ligands aminocaproic acid (AA). AA contains both an amine and a carboxyl group that can regulate the interactions between NCs and direct their anisotropic growth. Our growth method involves firstly the prepration of $CsPbBr_3$ NCs following a conventional hot-injection method.[1, 6, 11] After the induction of surface defects through solvent wash and the introduction of ligand AA, highly crystalline $CsPbBr_3$ NWs were obtained with widths in the range of 30–60 nm and lateral dimensions of up to several μm **(Figure 1)**. The mechanism by which the bidentate ligands induced the directed anisotropic growth of perovskite NWs was elucidated by transmission electron microscopy and PL studies. To the best of our knowledge, this work describes the first strategy for controllable growth of $CsPbBr_3$ perovskite NWs from NCs using bidentate ligands.

Experimental Section

Synthesis of $CsPbBr_3$ Nanowires from Nanocrystals: $CsPbBr_3$ NCs were prepared following a previous procedure by using the oleic acid and oleylamine (OA/OAm) mixture.[1, 6, 11] The obtained crude NCs solution was directly washed by *n*-hexane/acetone mixture (8:2 by volume), and centrifuged at least three times. Subsequently, the centrifuged substrate was re-dispersed in toluene, and aminocaproic acid (AA) was injected while stirring. The NWs was formed after 6 h. The mixture was then washed with *n*-hexane and centrifuged three times. Finally, the product was collected for further testing. For comparison, control NW sample was also synthesized following a solution-based synthesis.[23] For the synthesis of $CsPbBr_3$ nanocrystals from AA, the ligands of OA/OAm mixture were replaced with aminocaproic acid (AA).

Fabrication of photodetectors: The photodetector devices were fabricated following our previous procedures.[29] Typically, the NW solution was dropping onto the gold-based interdigitated electrodes, of which the spacing between adjacent fingers was 75 μm. Afterwards, the obtained electrodes were kept at 80 °C in a vacuum oven before further characterization.

RESULTS AND DISCUSSION

As reported, the surface of perovskite nanocrystals is dynamically capped with either oleylammonium bromide or oleylammonium oleate, which are very labile and sensitive to the external environment.[15-16, 30-31] Artificial surface defects are generated when detaching the surface dynamic ligands, which facilitate the reconstruction of the nanocrystals into various morphologies.[15, 21, 32]

To prove our hypothesis, we prepared $CsPbBr_3$ NCs following a previously reported hot-injection method by using oleic acid (OA) and olelylamine (OAm) as the passivating ligands.[1] **Figure 1a** shows the transmission electron microscopy (TEM) image of the obtained $CsPbBr_3$ NCs capped with OA/OAm. Typical cubic profiles with an average size of 7.1 nm were clearly observed by TEM analysis **(Figure 1a and c)**, consistent with previously reported results.[1, 11] The NCs displayed the typical close-packed nanocubic pattern due to strong interactions between the surface OA/OAm ligands. For comparison, we have also synthesized $CsPbBr_3$ NCs by using AA instead of OA/OAm as the ligands. The obtained nanocubes have well-defined edges with lengths of 10.2 nm, slightly larger than the $CsPbBr_3$ nanocubes obtained from OA/OAm mixtures (7.1 nm) (**Figure S2a**).

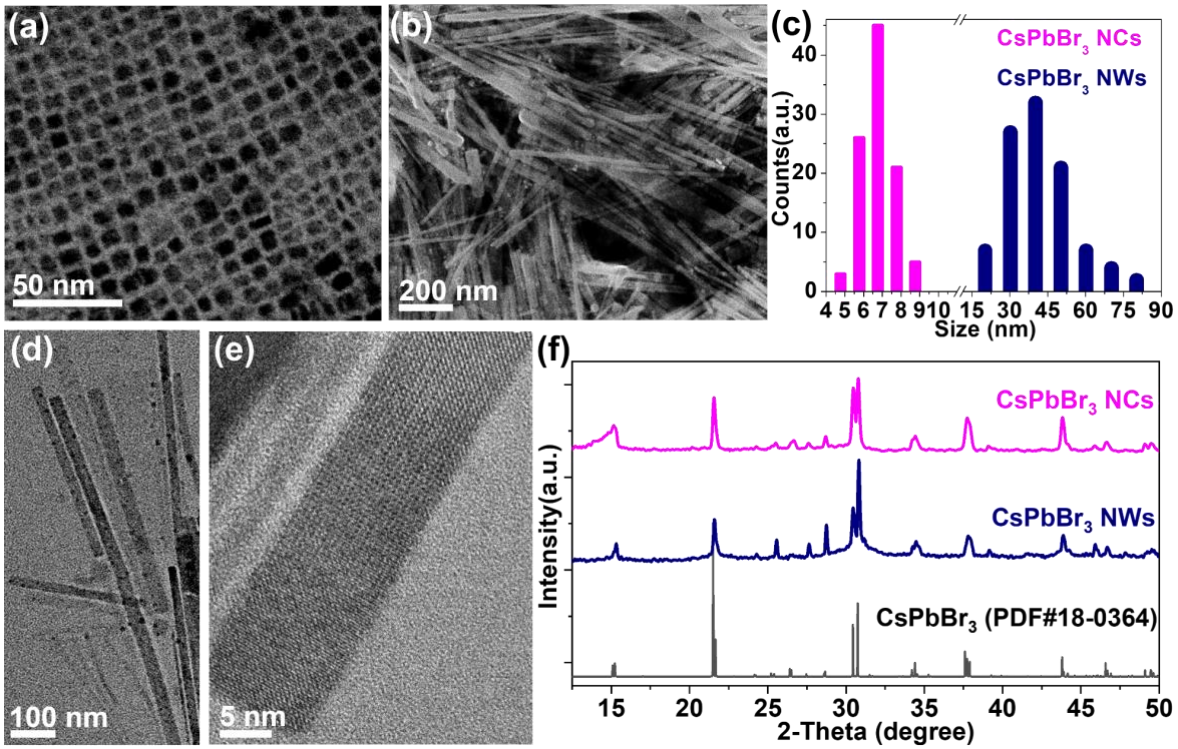

Figure 1. (a) Transmission electron microscope (TEM) image of $CsPbBr_3$ NCs. (b) Scanning electron microscope (SEM) image of as-formed $CsPbBr_3$ NWs. (c) Histograms of the size distributions of $CsPbBr_3$ NCs and the obtained NWs. TEM (d) and high-resolution TEM images (e) of the obtained $CsPbBr_3$ NWs. (f) XRD patterns of $CsPbBr_3$ NCs and NWs, as well as the PDF standard.

The crude NCs solution was washed by a hexane/acetone mixture to remove the excess ligands.[33] Compared with the initial well-defined cubic profile and close-packed pattern of NCs (7.1 nm, **Figure 1a**), the morphology and size of the $CsPbBr_3$ NCs remained unchanged after washing by hexane/acetone. The average distance between closely-packed NCs became much larger, and the spatial arrangement became irregular **(Figure S1a)**. Furthermore, after storing for 1 h, some irregular NCs aggregates were observed, possibly because defects on the NCs induced aggregation and reconstruction involving neighboring particles **(Figure S1)**. The aggregates grew into crystals larger than 100 nm after 6 h **(Figure S1)**. This morphology transformation further verified our hypothesis that the highly dynamic ligands on $CsPbBr_3$ NC can be dissociated from the surface by polar solvents to yield an artificially defective surface.[31, 33] Therefore, the as-washed NCs retained their cubic shape and size but showed a more irregular

distribution that originated from reduced interactions between the remaining ligands. Due to the high ion mobility, the defective crystal facets were prone to recombine with those on nearby nanocrystals, and consequently,they were reconstructed into larger crystals, similar to Ostwald ripening **(Figure S1)**.[34]

To circumvent the defect-induced, random crystal reconstruction and to realize controlled growth, we conceived an oriented reconstruction method based on the synergistic defect-bidentate ligand interactions. The introduced bidentate AA ligands occupied defect sites and altered the trajectory of the oriented fusion between neighboring nanocrystals. In the presence of AA (1%), nearly defect-free single-crystalline NWs were obtained with an average width of 35 nm and length of up to 10 μm after stirring for 6 h **(Figure 1b-d)**. These were similar to $CsPbBr_3$ NWs obtained from solution-based synthesis.[23]

The crystallinity of the NWs was confirmed by high-resolution TEM (HR-TEM) with an interplanar spacing of 5.8 Å, which was consistent with the (001) crystal lattice planes **(Figure 1e)**. Powder X-ray diffraction (PXRD) was further employed to verify the bulk crystallinity of the NCs**(Figure 1f)**. Strong peaks could be clearly observed, corresponding to the standard orthorhombic phase of $CsPbBr_3$ NCs (PDF# 18-0364). In addition, the PXRD of the obtained NWs showed the same diffraction pattern as that of the NCs, indicating that the crystal structure was preserved during the transformation.

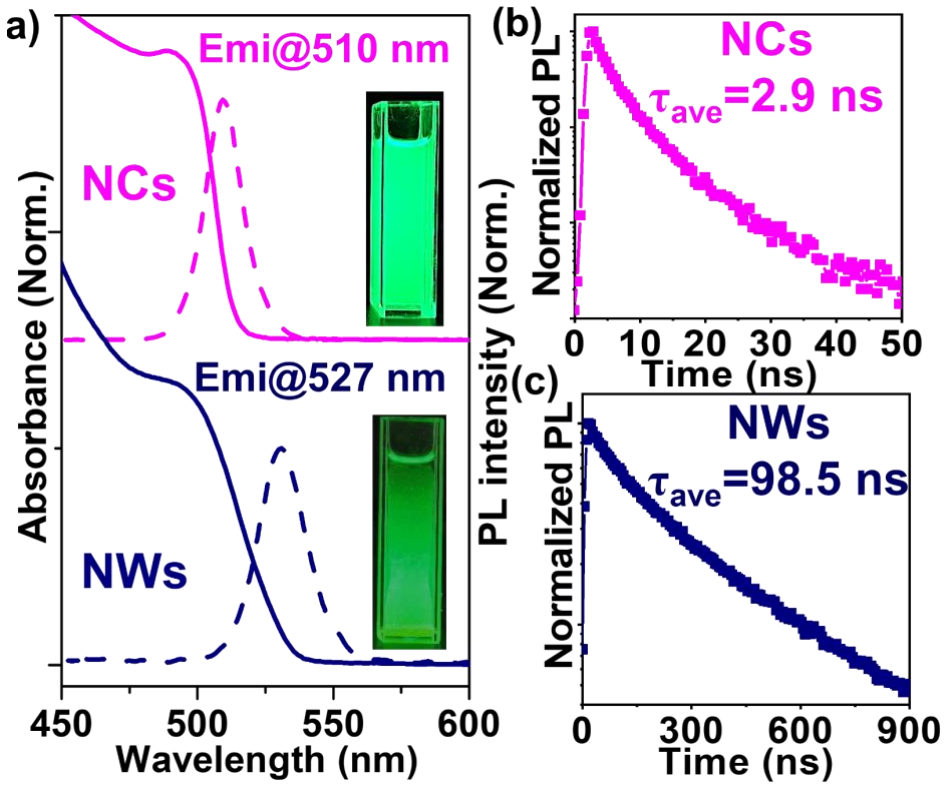

Figure 2. (a) Optical absorption (UV-vis) and PL emission spectra of $CsPbBr_3$ NCs and NWs. Insets in (a): Photographs of the $CsPbBr_3$ NC and NW solutions under UV light. PL lifetime measurements of $CsPbBr_3$ NCs (b) and NWs (c).

UV-vis absorption and photoluminescence (PL) measurements were conducted to study the optical properties of the $CsPbBr_3$ NCs and NWs. The colloid $CsPbBr_3$ NCs exhibited bright green fluorescence (inset in **Figure 2a**), a sharp PL emission peak at 510 nm, and an absorption onset at 508 nm**(Figure 2a)**, as well as a high PLQY of 87%. However, for the $CsPbBr_3$ NWs, an obvious red shift (~15 nm) in the respective emission and absorption peaks at 527 nm and 525 nm was observed **(Figure 2a)**. The NWs exhibited a much lower PLQY (59%), as shown by the weak fluorescence in the optical image (inset in **Figure 2a)**. The time-resolved PL decays of $CsPbBr_3$ NWs and NCs were compared. The NCs showed a PL carrier lifetime of ~2.9 ns **(Figure 2b)**, slightly shorter than that of the NCs from AA (~3.2 ns), whereas the NWs displayed a nearly 2 orders of magnitude higher PL lifetime of 98.5 ns **(Figure 2c and S2)**. This difference corroborates a much longer carrier diffusion length and appreciable photon

recycling within the highly crystalline $CsPbBr_3$ NWs capped with AA.[28]

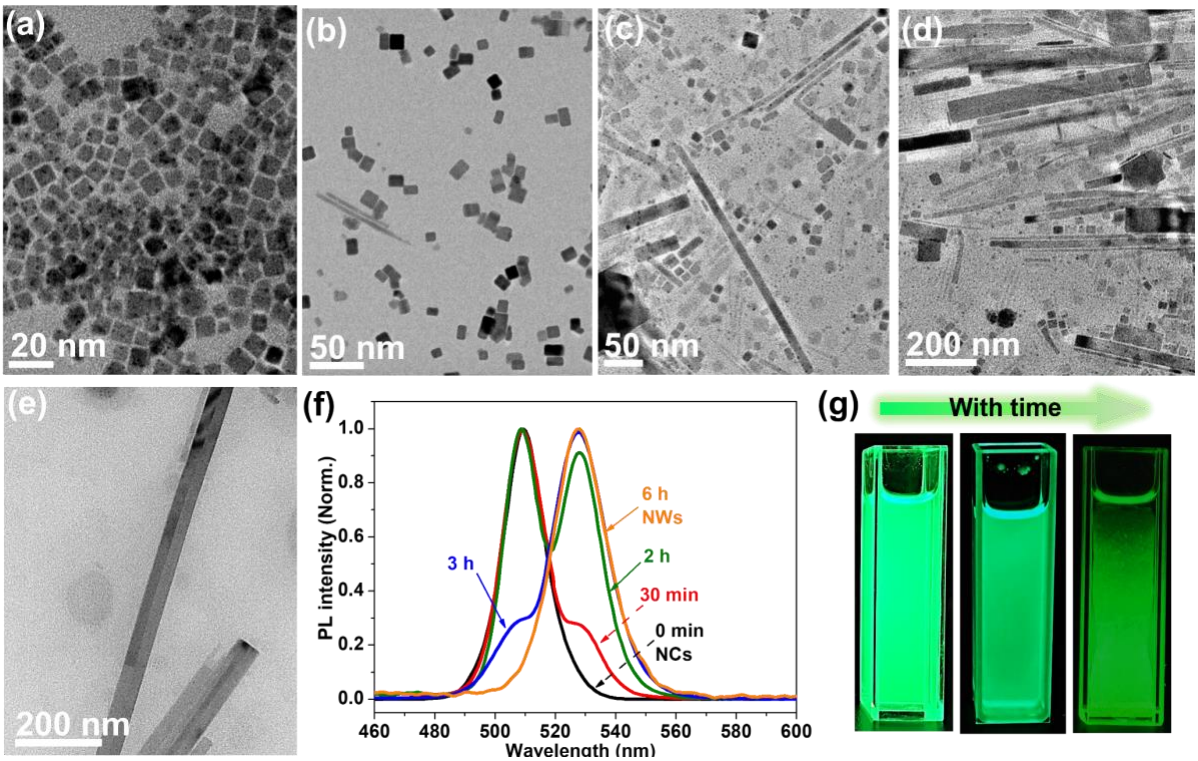

Figure 3. TEM images of the $CsPbBr_3$ NCs after washing (a) and the injection of ligand AA for 30 min (b), 2 h (c), 3 h (d), and 6 h (e). Optical PL evolution (f) of $CsPbBr_3$ NCs to NWs after solvent wash and injection of AA over time. (g) Photographs of the $CsPbBr_3$ NC solutions (0 min) and NW solutions (2 h and 6 h) under UV light.

As discussed above, the NWs were obtained from NCs after washing and reconstruction by injecting the bidentate ligand AA. Further TEM studies were carried out to reveal the shape evolution mechanism. **Figure 3a-e** shows the shape evolution of the washed $CsPbBr_3$ NCs after injecting AA. Consistent with aforementioned observations, the morphology and size of the washed $CsPbBr_3$ NCs remained unchanged compared with fresh NCs, while the average interparticle distance between the closely-packed NCs became much larger, and the spatial arrangement became irregular **(Figure 3a and S1).** After injecting AA, small aggregates of NCs could be detected in 30 min **(Figure 3b)**. The degree of oriented aggregation increased over time, as evidenced by the appearance of more NWs in 2 h **(Figure 3c)**, majority and longer NWs in 3 h **(Figure 3d)**, and eventually all longer NWs in 6 h **(Figure 3e)**, respectively. Further

sampling the SEM and TEM images at different locations also proved the shape evolution of $CsPbBr_3$ NCs to NWs **(Figure S3)**. The PL spectroscopic evolution of $CsPbBr_3$ NCs into NWs was shown in **Figure 3f**. The fresh NCs emitted bright green light (PL emission peak at 510 nm) with a high PLQY value (87%). After AA injection for 30 min, a shoulder peak at 527 nm appeared, along with a main peak at 510 nm. The peak at 527 nm became stronger after 2 h, and predominant at 3 h. The PL emission peak at 527 nm corresponded to the final $CsPbBr_3$ NWs **(Figure 3f)**. The PL evolution was also confirmed by the optical images under UV light (snapshots in **Figure 3g**).

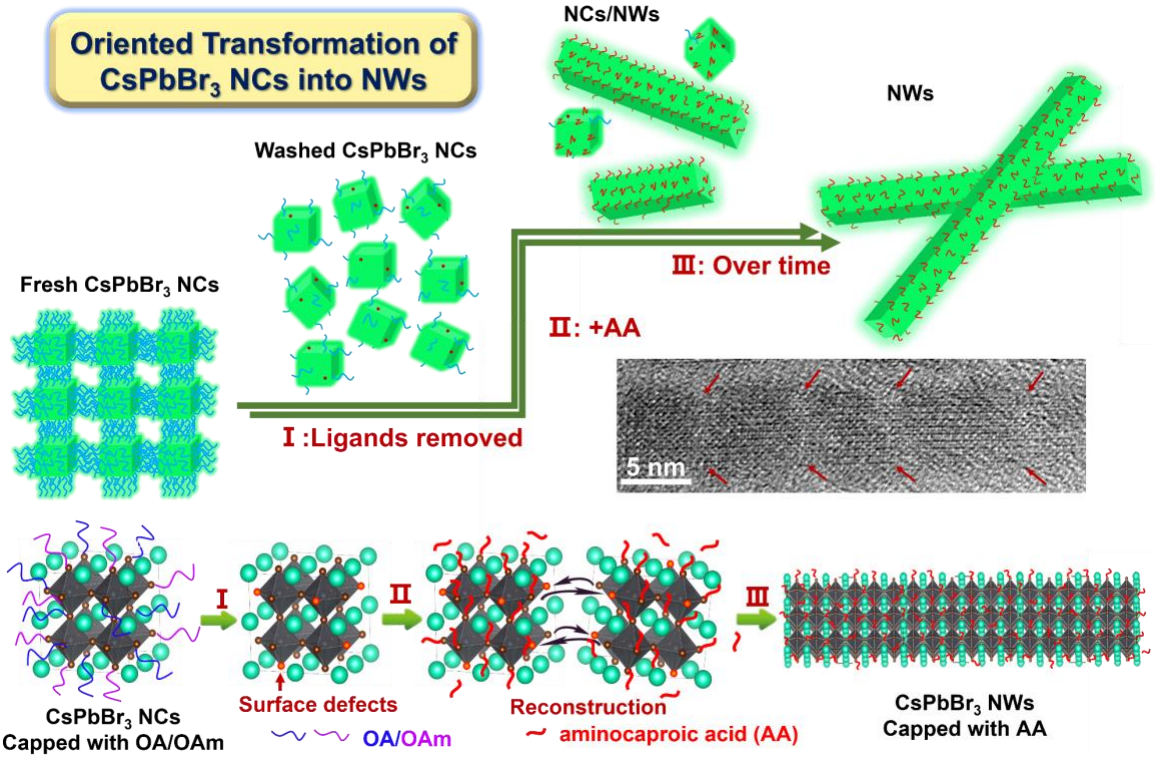

Figure 4. Schematic illustration of the shape evolution mechanism of the $CsPbBr_3$ NCs into NWs. Inset image shows the interfaces between several $CsPbBr_3$ NCs with oriented attachment.

The time-lapse morphology changes indicated that AA played a deterministic role in mediating the oriented growth of $CsPbBr_3$ NWs. We propose that such a shape change is mainly ascribed to the synergy between dynamic defect formation and reversible ligand attachment mediated by the bidentate AA, which directed the transformation and growth. The surface ligands on $CsPbBr_3$ NCs were highly dynamic and selectively adhered to certain crystal facets

via electrostatic and hydrophobic interactions. After washing with a polar solvent (hexane/acetone), a great fraction of surface ligands was removed, leaving a low density of ligands on the surface of NCs, together with more surface defects. The Pb/Br ratio of the $CsPbBr_3$ NCs determined by X-ray photoelectron spectroscopy (XPS) changed from 1:3.13 (fresh NCs) to 1:2.71 (NCs after washing), further indicating the defect (Br vacancy) formation. As reported, the defect formation energy on different crystal planes is different (for example, the defect formation energy of the $CsPbBr_3$ (110) surface is much larger than that of the (100) surface), thus yielding different surface defect densities ($CsPbBr_3$ (100) surface has a larger density of defects than (110) surface).[21] The amine, carboxylic acid and ammonium groups presented different bonding energies towards different crystal planes. After introducing AA, the ligands bound to the surface defects on specific crystal facets, creating an anisotropic growth environment,[21] which altered the interactions and equilibrium between re-attached ligands AA, as illustrated in **Figure 4**. Therefore, oriented attachment favoring specific crystal facets occurred, leading to directional growth.[21, 35] The bidentate AA ligands facilitate the "crosslinking" of the NCs, while higher growth rates on specific crystal planes leads to the oriented growth of anisotropic NWs rather than Ostwald ripening.[34] The oriented-attachment transformation was verified by the step-edges in large NCs observed by TEM **(Figure 4 and S4)**. The inter-particle distance decreased concurrently with lattice fusion between NCs, which further supported our hypothesis that the high ion mobility would induce the reconstruction of defective crystal facets to produce larger crystals over time **(Figure 4)**.

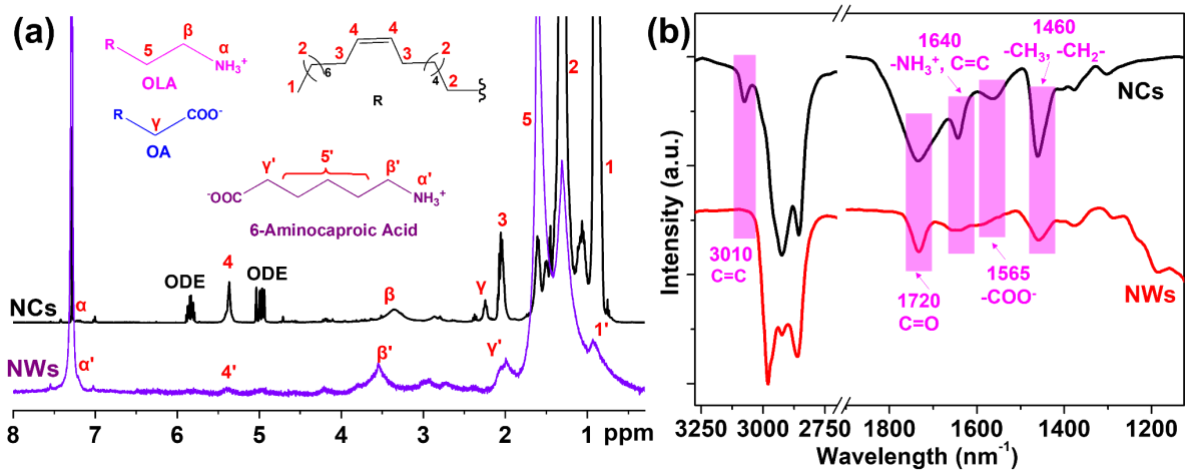

Figure 5. (a) ^{1}H NMR spectra (toluene-*d*), and (b) Infrared spectra of the $CsPbBr_3$ NCs and NWs.

As reported, the surface-bound species on $CsPbBr_3$ NCs are closely related to the size and shape of the nanocrystals, as well as their corresponding optical properties. Therefore, ^{1}H NMR and infrared (IR) spectroscopy were acquired to investigate the chemical structures of the surface species of $CsPbBr_3$ NCs and NWs . In the ^{1}H NMR spectrum of the $CsPbBr_3$ NCs (OA/OAm combination), the resonances corresponding to the surface-bound oleate and ammonium species could be assigned accordinlgy, with a very characteristic alkene peak at 5.50 ppm that showed the presence of oleates **(Figure 5a)**. For the $CsPbBr_3$ NWs, the peak at 5.50 ppm (label 4') nearly disappeared, indicating that the surface-bound primal species was removed. Peaks at 7.2 ppm (α'), 3.4 ppm (β'), and 2.2 ppm (γ') could be observed, accompanied by lower-intensity peaks at 2.1 ppm (3) and 0.9 ppm (1), further indicating that the surface was occupied by AA.

Figure 5b shows the IR spectra of $CsPbBr_3$ NCs and NWs. In the NC spectrum, the characteristic C=C stretching and bending vibration signals can be clearly detected at 3010 and 1640 cm^{-1}, along with intense absorptions at 1460, 1565, 1640, 1720, and 2950–2850 cm^{-1}, which were attributed to C-H bending, $-COO^{-}$ stretching, $-NH_3^{+}$ deformation, C=O stretching, and C-H stretching vibrations of the OA and OAm, respectively. However, for the NWs, theC=C stretching and bending vibration signals (3010 and 1640 cm^{-1}), and the C-H bending vibration peak (1460 cm^{-1}) decreased dramatically, implying that the surface oleate ligands

were replaced by AA. Furthermore, the O−C=O peak at 288 eV of the C 1*s* high-resolution XPS spectrum of NWs became stronger than that of the NCs, further corroborating that the NWs were capped with AA **(Figure S5)**. All of the above analysis supported that defects and the bidentate AA ligands are essential for transforming NCs to NWs.

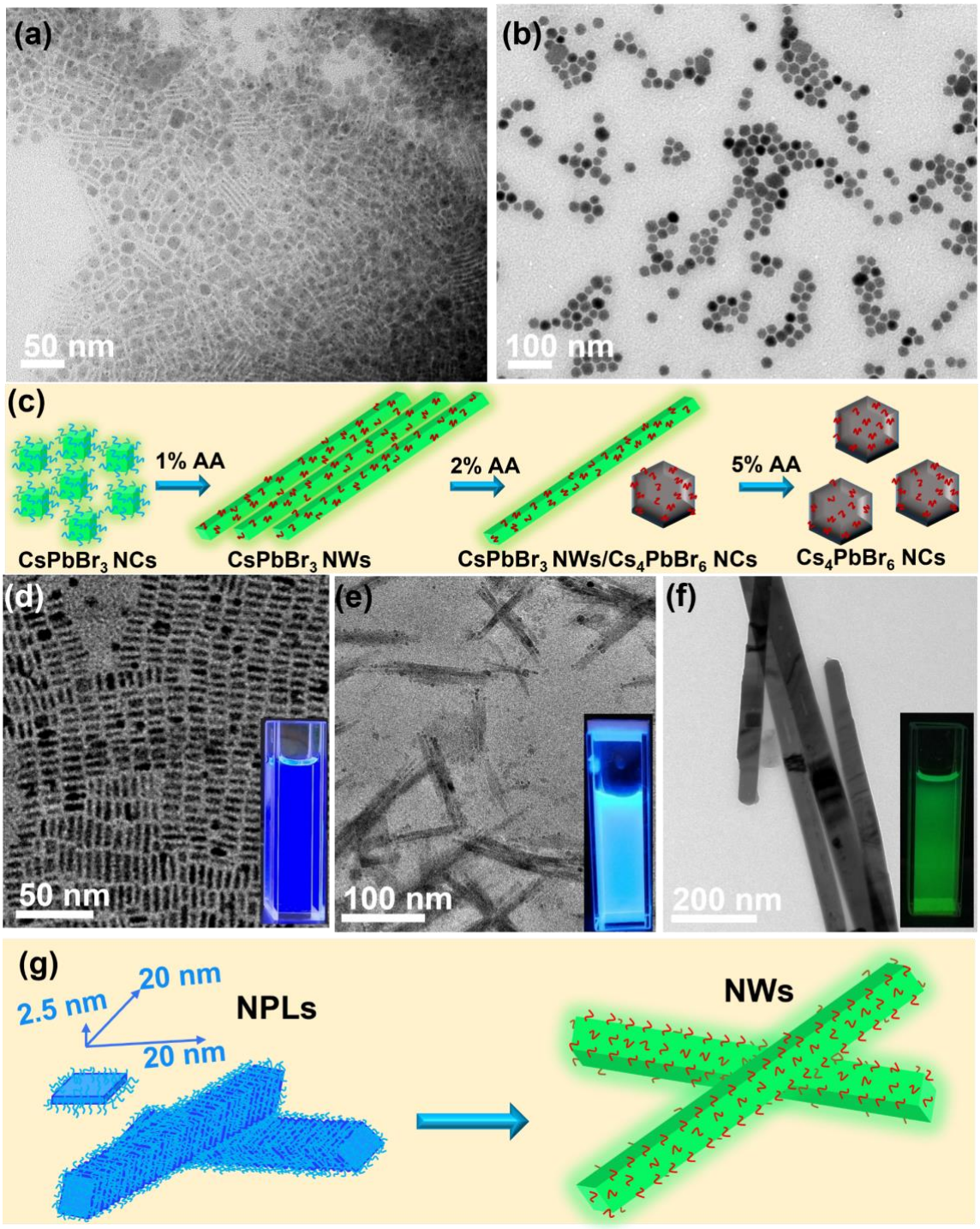

Figure 6. TEM images of the obtained $CsPbBr_3$ NCs with 2% AA (a) and 5% AA (b) for 6 h, $CsPbBr_3$ NPLs (d), with 1% AA for 3 h (e) and 6 h (f). (c) and (g) Schematic illustrations of the corresponding

morphological transformation. Insets in (d-f): photographs of the $CsPbBr_3$ NPL and NW solutions under UV light (λ = 365 nm).

To provide further insight into the effect of bidentate ligands on NWs growth from NCs, we tracked the morphologies upon changing the amount of AA. **Figure 6a** shows the TEM image of the final morphology after introducing 2% AA. In addition to NWs, hexagon-shaped nanocrystals in the size of 20–30 nm could also be clearly observed. Comparing the XRD pattern to that of orthorhombic $CsPbBr_3$ NCs revealed several additional peaks, which were indexed to the rhombohedral phase of Cs_4PbBr_6 (PDF# 01-073-2478) **(Figure S6)**.[36-37] Therefore, the hexagonal nanocrystals were assigned as Cs_4PbBr_6 NCs. No NWs were detected, and only Cs_4PbBr_6 NCs with sizes of 20–30 nm could be observed when using 5% AA. This result indicates the obvious phase transformation from $CsPbBr_3$ to Cs_4PbBr_6 NCs as increasing the content of AA. Such a phase transformation can be rationalized by the tight binding between AA and $PbBr_2$, which causes further leaching of $PbBr_2$ from $CsPbBr_3$ NCs and initiates a diffusion-recrystallization process. A similar process was observed when excessive amine was used to induce phase transformations.[32, 38] We further measured the morphologies of the nanoparticles after changing the bidentate ligands from AA to adipic acid and hexamethylenediamine **(Figure S7)**. Interestingly, some irregular nanoplatelets were obtained when using adipic acid (20–50 nm), and 20–30 nm Cs_4PbBr_6 NCs were detected with hexamethylene diamine. This further implied that both the acid and amine groups in bidentate ligands played essential roles in regulating the anisotropic growth of the nanocrystals along a certain direction.

We also confirmed that the synergistic defect and bidentate ligand-driven oriented reconstruction mechanism could be applied to nanoplatelets (NPLs). TEM was employed to track the morphology evolution from NPLs to NWs (**Figure 6d-g**). **Figure 6d** showed a typical quasi-2D structure featuring NPLs with an edge length of ~12.9 nm and a thickness of ~2.5 nm.

Benefitting from the strong interactions between the ligands, the NPLs exhibited a *face-to-face* close-packed structure. After being washed and injected with AA for 3 h, the nanosheets transformed into longer NWs (**Figure 6e**). **Figure 6f** shows the final $CsPbBr_3$ NWs after 6 h, with a width of 50 nm. The corresponding transformations were further confirmed by the morphologies and PL spectra **(Figure S8)**. The emission peaks shifted from 475 nm (blue) for the NPLs to 527 nm (green) for the NWs.

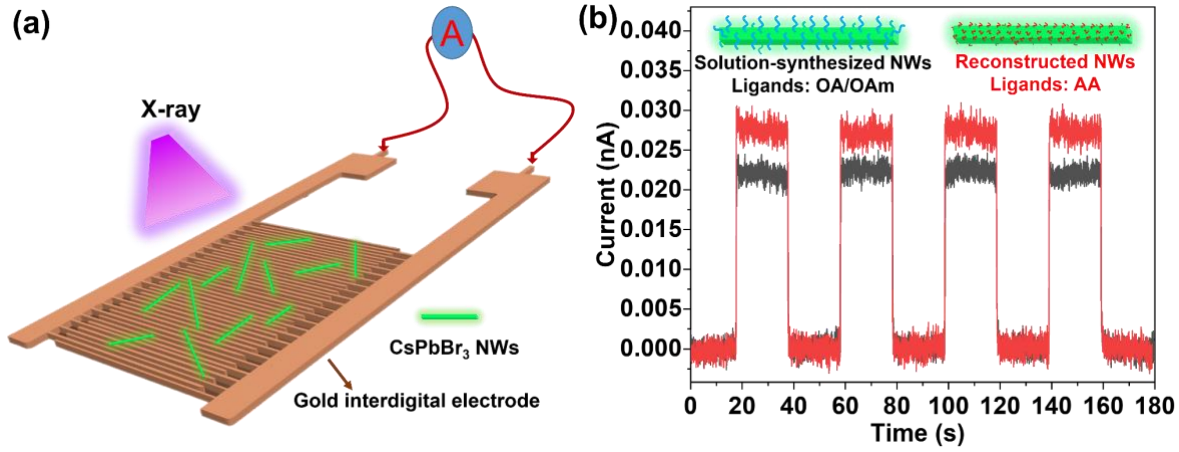

Figure 7. (a) Schematic of the fabricated photodetector based on $CsPbBr_3$ NWs (the interdigital distance of the electrodes was 75 μm). (b) Photocurrent response of devices based on $CsPbBr_3$ NWs from solution-based synthesis (capped with OA/OAm) and reconstructed synthesis (capped with AA) under X-ray illumination (a bias voltage of 1 V).

$CsPbX_3$ NWs have several merits, including high crystallinity, high aspect ratios, strong light absorption, and large carrier diffusion lengths. They accordingly display superior sensitivity to light in nano-devices, which motivates us to explore their potential applications as photodetectors. We fabricated photodetectors by dropping $CsPbBr_3$ NWs solution onto gold interdigitated electrodes (interdigital spacing: 75 μm), as shown in **Figure 7a** and **S9**.[29, 39] $CsPbBr_3$ NWs obtained from solution-based synthesis (capped with OA/OAm) and fresh NCs were also prepared and integrated into similar devices.[1, 11, 23] However, we could not obtain a working $CsPbBr_3$ NCs-based device due to the poor continuity of $CsPbBr_3$ NCs. When the electrodes were operated under an external electric field, the electron-hole pairs formed in NWs

from X-ray radiation were rapidly separated and collected by the Au-electrodes.

We evaluated the current-time (*I-T*) characteristics of the devices under X-ray illumination. In response to on/off cycles, both NWs promptly generated photocurrents with reproducible characteristics. The device from the reconstructed NWs displayed a significant photocurrent enhancement (2.75×10^{-11} A) compared with that from the solution-synthesized NWs (2.28×10^{-11} A) under a 1 V bias. Moreover, the photodetector based on reconstructed $CsPbBr_3$ NWs exhibited a very fast rise time (22 ms), shorter than that of the solution-synthesized NWs (28 ms), as shown in **Figure S9b**. This further indicates that the re-constructed $CsPbBr_3$ NWs showed a more sensitive photoelectric response. Besides, the photocurrent of the device of interest increased with the increase of radiation dose rates from 100 to 300 μA (0.053 to 0.082 $\mu Gy_{air}\ s^{-1}$),[39] as well as the increasing working bias (0.01 to 1 V). In addition, such device displayed a high stability, as indicated by a minimal decrease of photocurrent after storing for 2 months (**Figure S9e)**. Overall, the $CsPbX_3$ NW-based photodetector devices have exhibited excellent photoelectric response properties (high sensitivity, reproducibility and stability), which will greatly expand their application in optoelectronic devices.

Conclusion

We have demonstrated a new method that uses defects and a bidentate AA ligand to direct the synthesis of $CsPbBr_3$ NWs from $CsPbBr_3$ NCs. With the assistance of defects and bidentate ligands, the ~7 nm $CsPbBr_3$ NCs could be reconstructed into NWs with 20–60 nm widths and several micrometers in length within 6 h. The obtained NWs exhibited a sharp PL peak at 527 nm, a PLQY of 69%, and a PL lifetime of 98.5 ns. Such protocol is also effective in inducing the anisotropic growth of perovskite NCs from NPLs, proving its versatility. Devices based on reconstructed $CsPbBr_3$ NWs displayed more sensitive photoresponses to X-ray illumination

than the ones based on solution-synthesized NWs. This work offers an effective and promising approach for the construction of diverse structures by changing the surface/interfacial chemistry of perovskites for optoelectronic applications.

Supporting Information

General chemical information, experimental details, and characterization methods; SEM, TEM, XPS and XRD of $CsPbBr_3$ NCs, the obtained NWs, NPLs, and Cs_4PbBr_6 NCs; Schematic of the interdigital electrodes; Photocurrent response of the fabricated devices. This material is available free of charge via the Internet at XXX.

AUTHOR INFORMATIONAuthor Contributions

All authors have given approval to the final version of the manuscript.

Notes

The authors declare no competing financial interest.

Acknowledgments

This work was primarily supported by the National Natural Science Foundation of China (NSFC Grants 52172153, 51802254) and National Key Research and Development Project (No. 2019YFB2004303). Y.L. acknowledges the support from Molecular Foundry, which was supported by the Office of Science, Office of Basic Energy Sciences, of the U.S. Department of Energy under Contract No. DE-AC02-05CH11231.

REFERENCES

(1) Protesescu, L.; Yakunin, S.; Bodnarchuk, M. I.; Krieg, F.; Caputo, R.; Hendon, C. H.; Yang, R. X.; Walsh, A.; Kovalenko, M. V. Nanocrystals of Cesium Lead Halide Perovskites ($CsPbX_{(3)}$, X = Cl, Br, and I): Novel Optoelectronic Materials Showing Bright Emission with Wide Color Gamut. *Nano Lett.* **2015,** *15* (6), 3692-3696.
(2) Akkerman, Q. A.; D'Innocenzo, V.; Accornero, S.; Scarpellini, A.; Petrozza, A.; Prato, M.; Manna, L. Tuning the Optical Properties of Cesium Lead Halide Perovskite Nanocrystals by Anion Exchange Reactions. *J. Am. Chem. Soc.* **2015,** *137* (32), 10276-10281.
(3) Song, J.; Li, J.; Li, X.; Xu, L.; Dong, Y.; Zeng, H. Quantum Dot Light-Emitting Diodes

Based on Inorganic Perovskite Cesium Lead Halides ($CsPbX_3$). *Adv. Mater.* **2015,** *27* (44), 7162-7167.
(4) Wang, H.; Kim, D. H. Perovskite-based Photodetectors: Materials and Devices. *Chem. Soc. Rev.* **2017,** *46* (17), 5204-5236.
(5) Seo, H. K.; Kim, H.; Lee, J.; Park, M. H.; Jeong, S. H.; Kim, Y. H.; Kwon, S. J.; Han, T. H.; Yoo, S.; Lee, T. W. Efficient Flexible Organic/Inorganic Hybrid Perovskite Light-Emitting Diodes Based on Graphene Anode. *Adv. Mater.* **2017,** *29* (12), 1605587.
(6) Almeida, G.; Goldoni, L.; Akkerman, Q.; Dang, Z.; Khan, A. H.; Marras, S.; Moreels, I.; Manna, L. Role of Acid-Base Equilibria in the Size, Shape, and Phase Control of Cesium Lead Bromide Nanocrystals. *ACS Nano* **2018,** *12* (2), 1704-1711.
(7) Akkerman, Q. A.; Motti, S. G.; Srimath Kandada, A. R.; Mosconi, E.; D'Innocenzo, V.; Bertoni, G.; Marras, S.; Kamino, B. A.; Miranda, L.; De Angelis, F.; Petrozza, A.; Prato, M.; Manna, L. Solution Synthesis Approach to Colloidal Cesium Lead Halide Perovskite Nanoplatelets with Monolayer-Level Thickness Control. *J. Am. Chem. Soc.* **2016,** *138* (3), 1010-1016.
(8) Koscher, B. A.; Swabeck, J. K.; Bronstein, N. D.; Alivisatos, A. P. Essentially Trap-Free $CsPbBr_3$ Colloidal Nanocrystals by Postsynthetic Thiocyanate Surface Treatment. *J. Am. Chem. Soc.* **2017,** *139* (19), 6566-6569.
(9) Dutta, A.; Behera, R. K.; Pal, P.; Baitalik, S.; Pradhan, N. Near-Unity Photoluminescence Quantum Efficiency for All $CsPbX_3$ (X=Cl, Br, and I) Perovskite Nanocrystals: A Generic Synthesis Approach. *Angew. Chem. Int. Ed.* **2019,** *58* (17), 5552-5556.
(10) Zhang, Q.; Yin, Y. All-Inorganic Metal Halide Perovskite Nanocrystals: Opportunities and Challenges. *ACS Cent. Sci.* **2018,** *4* (6), 668-679.
(11) Pan, A.; He, B.; Fan, X.; Liu, Z.; Urban, J. J.; Alivisatos, A. P.; He, L.; Liu, Y. Insight into the Ligand-Mediated Synthesis of Colloidal $CsPbBr_3$ Perovskite Nanocrystals: The Role of Organic Acid, Base, and Cesium Precursors. *ACS Nano* **2016,** *10* (8), 7943-7954.
(12) Dutta, A.; Behera, R. K.; Dutta, S. K.; Das Adhikari, S.; Pradhan, N. Annealing $CsPbX_3$ (X = Cl and Br) Perovskite Nanocrystals at High Reaction Temperatures: Phase Change and Its Prevention. *J. Phys. Chem. Lett.* **2018,** *9* (22), 6599-6604.
(13) Dong, Y.; Qiao, T.; Kim, D.; Parobek, D.; Rossi, D.; Son, D. H. Precise Control of Quantum Confinement in Cesium Lead Halide Perovskite Quantum Dots via Thermodynamic Equilibrium. *Nano Lett.* **2018,** *18* (6), 3716-3722.
(14) Sun, S.; Yuan, D.; Xu, Y.; Wang, A.; Deng, Z. Ligand-Mediated Synthesis of Shape-Controlled Cesium Lead Halide Perovskite Nanocrystals via Reprecipitation Process at Room Temperature. *ACS Nano* **2016,** *10* (3), 3648-3657.
(15) De Roo, J.; Ibanez, M.; Geiregat, P.; Nedelcu, G.; Walravens, W.; Maes, J.; Martins, J. C.; Van Driessche, I.; Kovalenko, M. V.; Hens, Z. Highly Dynamic Ligand Binding and Light Absorption Coefficient of Cesium Lead Bromide Perovskite Nanocrystals. *ACS Nano* **2016,** *10* (2), 2071-2081.
(16) Kim, Y.; Yassitepe, E.; Voznyy, O.; Comin, R.; Walters, G.; Gong, X.; Kanjanaboos, P.; Nogueira, A. F.; Sargent, E. H. Efficient Luminescence from Perovskite Quantum Dot Solids. *ACS Appl. Mater. Interfaces* **2015,** *7* (45), 25007-25013.
(17) Parobek, D.; Dong, Y.; Qiao, T.; Rossi, D.; Son, D. H. Photoinduced Anion Exchange in Cesium Lead Halide Perovskite Nanocrystals. *J. Am. Chem. Soc.* **2017,** *139* (12), 4358-4361.
(18) Huang, H.; Bodnarchuk, M. I.; Kershaw, S. V.; Kovalenko, M. V.; Rogach, A. L. Lead Halide Perovskite Nanocrystals in the Research Spotlight: Stability and Defect Tolerance. *ACS Energy Lett.* **2017,** *2* (9), 2071-2083.
(19) Akkerman, Q. A.; Raino, G.; Kovalenko, M. V.; Manna, L. Genesis, Challenges and Opportunities for Colloidal Lead Halide Perovskite Nanocrystals. *Nat. Mater.* **2018,** *17* (5), 394-405.

(20) Li, P.; Yang, D.; Tan, Y.; Cao, M.; Zhong, Q.; Chen, M.; Hu, H.; Sun, B.; Xu, Y.; Zhang, Q. Consecutive Interfacial Transformation of Cesium Lead Halide Nanocubes to Ultrathin Nanowires with Improved Stability. *ACS Appl. Mater. Interfaces* **2019,** *11* (3), 3351-3359.
(21) Pan, J.; Li, X.; Gong, X.; Yin, J.; Zhou, D.; Sinatra, L.; Huang, R.; Liu, J.; Chen, J.; Dursun, I.; El-Zohry, A. M.; Saidaminov, M. I.; Sun, H. T.; Mohammed, O. F.; Ye, C.; Sargent, E. H.; Bakr, O. M. Halogen Vacancies Enable Ligand-Assisted Self-Assembly of Perovskite Quantum Dots into Nanowires. *Angew. Chem. Int. Ed.* **2019,** *58* (45), 16077-16081.
(22) Hudait, B.; Dutta, S. K.; Patra, A.; Nasipuri, D.; Pradhan, N. Facets Directed Connecting Perovskite Nanocrystals. *J. Am. Chem. Soc.* **2020,** *142* (15), 7207-7217.
(23) Zhang, D.; Eaton, S. W.; Yu, Y.; Dou, L.; Yang, P. Solution-Phase Synthesis of Cesium Lead Halide Perovskite Nanowires. *J. Am. Chem. Soc.* **2015,** *137* (29), 9230-9233.
(24) Brennan, M. C.; Forde, A.; Zhukovskyi, M.; Baublis, A. J.; Morozov, Y. V.; Zhang, S.; Zhang, Z.; Kilin, D. S.; Kuno, M. Universal Size-Dependent Stokes Shifts in Lead Halide Perovskite Nanocrystals. *J. Phys. Chem. Lett.* **2020,** *11* (13), 4937-4944.
(25) Tong, Y.; Bohn, B. J.; Bladt, E.; Wang, K.; Muller-Buschbaum, P.; Bals, S.; Urban, A. S.; Polavarapu, L.; Feldmann, J. From Precursor Powders to $CsPbX_3$ Perovskite Nanowires: One-Pot Synthesis, Growth Mechanism, and Oriented Self-Assembly. *Angew. Chem. Int. Ed.* **2017,** *56* (44), 13887-13892.
(26) Huang, L.; Gao, Q.; Sun, L. D.; Dong, H.; Shi, S.; Cai, T.; Liao, Q.; Yan, C. H. Composition-Graded Cesium Lead Halide Perovskite Nanowires with Tunable Dual-Color Lasing Performance. *Adv. Mater.* **2018,** *30* (27), e1800596.
(27) Zhai, W.; Lin, J.; Li, C.; Hu, S.; Huang, Y.; Yu, C.; Wen, Z.; Liu, Z.; Fang, Y.; Tang, C. Solvothermal Synthesis of Cesium Lead Halide Perovskite Nanowires with Ultra-high Aspect Ratios for High-performance Photodetectors. *Nanoscale* **2018,** *10* (45), 21451-21458.
(28) Liu, J.; Song, K.; Shin, Y.; Liu, X.; Chen, J.; Yao, K. X.; Pan, J.; Yang, C.; Yin, J.; Xu, L.-J.; Yang, H.; El-Zohry, A. M.; Xin, B.; Mitra, S.; Hedhili, M. N.; Roqan, I. S.; Mohammed, O. F.; Han, Y.; Bakr, O. M. Light-Induced Self-Assembly of Cubic $CsPbBr_3$ Perovskite Nanocrystals into Nanowires. *Chem. Mater.* **2019,** *31* (17), 6642-6649.
(29) Pan, A.; Ma, X.; Huang, S.; Wu, Y.; Jia, M.; Shi, Y.; Liu, Y.; Wangyang, P.; He, L.; Liu, Y. $CsPbBr_3$ Perovskite Nanocrystal Grown on MXene Nanosheets for Enhanced Photoelectric Detection and Photocatalytic CO_2 Reduction. *J. Phys. Chem. Lett.* **2019,** *10* (21), 6590-6597.
(30) Dey, A.; Ye, J.; De, A.; Debroye, E.; Ha, S. K.; Bladt, E.; Kshirsagar, A. S.; Wang, Z.; Yin, J.; Wang, Y.; Quan, L. N.; Yan, F.; Gao, M.; Li, X.; Shamsi, J.; Debnath, T.; Cao, M.; Scheel, M. A.; Kumar, S.; Steele, J. A.; Gerhard, M.; Chouhan, L.; Xu, K.; Wu, X. G.; Li, Y.; Zhang, Y.; Dutta, A.; Han, C.; Vincon, I.; Rogach, A. L.; Nag, A.; Samanta, A.; Korgel, B. A.; Shih, C. J.; Gamelin, D. R.; Son, D. H.; Zeng, H.; Zhong, H.; Sun, H.; Demir, H. V.; Scheblykin, I. G.; Mora-Sero, I.; Stolarczyk, J. K.; Zhang, J. Z.; Feldmann, J.; Hofkens, J.; Luther, J. M.; Perez-Prieto, J.; Li, L.; Manna, L.; Bodnarchuk, M. I.; Kovalenko, M. V.; Roeffaers, M. B. J.; Pradhan, N.; Mohammed, O. F.; Bakr, O. M.; Yang, P.; Muller-Buschbaum, P.; Kamat, P. V.; Bao, Q.; Zhang, Q.; Krahne, R.; Galian, R. E.; Stranks, S. D.; Bals, S.; Biju, V.; Tisdale, W. A.; Yan, Y.; Hoye, R. L. Z.; Polavarapu, L. State of the Art and Prospects for Halide Perovskite Nanocrystals. *ACS Nano* **2021,** *15* (7), 10775-10981.
(31) Wang, Y.; Li, X.; Sreejith, S.; Cao, F.; Wang, Z.; Stuparu, M. C.; Zeng, H.; Sun, H. Photon Driven Transformation of Cesium Lead Halide Perovskites from Few-Monolayer Nanoplatelets to Bulk Phase. *Adv. Mater.* **2016,** *28* (48), 10637-10643.
(32) Palazon, F.; Almeida, G.; Akkerman, Q. A.; De Trizio, L.; Dang, Z.; Prato, M.; Manna, L. Changing the Dimensionality of Cesium Lead Bromide Nanocrystals by Reversible Postsynthesis Transformations with Amines. *Chem. Mater.* **2017,** *29* (10), 4167-4171.
(33) Pan, A.; Wang, J.; Jurow, M. J.; Jia, M.; Liu, Y.; Wu, Y.; Zhang, Y.; He, L.; Liu, Y. General Strategy for the Preparation of Stable Luminous Nanocomposite Inks Using Chemically

Addressable $CsPbX_3$ Peroskite Nanocrystals. *Chem. Mater.* **2018,** *30* (8), 2771-2780.
(34) De Yoreo, J. J. V., P. G., Principles of Crystal Nucleation and Growth. *Reviews in Mineralogy and Geochemistry* **2003,** *54*, 57-93.
(35) Veldhuis, S. A.; Boix, P. P.; Yantara, N.; Li, M.; Sum, T. C.; Mathews, N.; Mhaisalkar, S. G. Perovskite Materials for Light-Emitting Diodes and Lasers. *Adv. Mater.* **2016,** *28* (32), 6804-6834.
(36) Zhang, Y.; Saidaminov, M. I.; Dursun, I.; Yang, H.; Murali, B.; Alarousu, E.; Yengel, E.; Alshankiti, B. A.; Bakr, O. M.; Mohammed, O. F. Zero-Dimensional Cs_4PbBr_6 Perovskite Nanocrystals. *J. Phys. Chem. Lett.* **2017,** *8* (5), 961-965.
(37) Seth, S.; Samanta, A. Fluorescent Phase-Pure Zero-Dimensional Perovskite-Related Cs_4PbBr_6 Microdisks: Synthesis and Single-Particle Imaging Study. *J. Phys. Chem. Lett.* **2017,** *8* (18), 4461-4467.
(38) Udayabhaskararao, T.; Houben, L.; Cohen, H.; Menahem, M.; Pinkas, I.; Avram, L.; Wolf, T.; Teitelboim, A.; Leskes, M.; Yaffe, O.; Oron, D.; Kazes, M. A Mechanistic Study of Phase Transformation in Perovskite Nanocrystals Driven by Ligand Passivation. *Chem. Mater.* **2017,** *30* (1), 84-93.
(39) Gou, Z.; Huanglong, S.; Ke, W.; Sun, H.; Tian, H.; Gao, X.; Zhu, X.; Yang, D.; Wangyang, P. Self-Powered X-Ray Detector Based on All-Inorganic Perovskite Thick Film with High Sensitivity Under Low Dose Rate. *Phys. Status Solidi – R.* **2019,** *13* (8), 1900094.

Table of Content Graphic